Journal of Materials Chemistry

Cite this: *J. Mater. Chem.*, 2011, **21**, 12034

www.rsc.org/materials

PAPER

Green and facile synthesis of highly biocompatible graphene nanosheets and its application for cellular imaging and drug delivery†‡

Kunping Liu,[ab] Jing-Jing Zhang,[a] Fang-Fang Cheng,[a] Ting-Ting Zheng,[a] Chunming Wang*[b] and Jun-Jie Zhu*[a]

Received 19th February 2011, Accepted 24th May 2011
DOI: 10.1039/c1jm10749f

A green and facile method for the preparation of gelatin functionalized graphene nanosheets (gelatin–GNS) was reported by using gelatin as a reducing reagent. Meanwhile, the gelatin also played an important role as a functionalized reagent to prevent the aggregation of the graphene nanosheets. The obtained biocompatible gelatin–GNS exhibited excellent stability in water and various physiological fluids including, cellular growth media as well as serum which were critical prerequisites for biomedicine application of graphene. Cellular toxicity test suggested that the gelatin–GNS was nontoxic for MCF-7 cells, even at a high concentration of 200 μg mL^{-1}. Furthermore, the anticancer drug was loaded onto the gelatin–GNS at a high loading capacity *via* physisorption for cellular imaging and drug delivery. The doxorubicin/gelatin–GNS composite exhibited a high toxicity to kill MCF-7 cells and experienced a gelatin-mediated sustained release *in vitro*, which has the potential advantage of increasing the therapeutic efficacy. Therefore, the gelatin–GNS could be selected as an ideal drug carrier to be applied in biomedicine studies.

1. Introduction

Graphene nanosheets (GNS), a flat monolayer of sp^2 hybridized carbon atoms which tightly packed into a two-dimensional honeycomb lattice, have attracted enormous attention since it was first reported in 2004,[1] due to its novel properties and potential application.[2–4] At present, great efforts have been made for the preparation of graphene nanosheets.[5–7] Among them, the chemical reduction of exfoliated graphene oxide (EGO) is the most commonly used approach due to its low cost for large scale preparation. However, the GNS is hydrophobic and tends to form agglomerates or even re-graphitized to graphite because of the Van der Waals interaction and strong π–π stacking between the GNS. Therefore, the prevention for aggregation is of great importance because most of the GNS unique properties are only associated with individual sheets.[8] For this purpose, covalent and noncovalent strategies have been used for the functionalization of GNS to overcome the aggregation by using polymers[9,10] or DNA[11] as a functionalization reagent. Unfortunately, the use of highly toxic reducing reagents of hydrazine may contaminate the acquired GNS and thereby hinder its further application. Recently, a novel strategy was developed to provide a nontoxic and environmental friendly approach for the preparation of soluble GNS,such as using L-ascorbic acid (AA),[12] reducing sugar[13] or bovine serum albumin (BSA)[14] as the reducing reagent as well as functionalization reagent. However, the long reaction time (48 h) or strong alkaline (pH 12) may hamper its application. Therefore, it is still a challenge to search for new bi-function reagents for the green and facile preparation of aqueous soluble GNS in neutral reaction conditions.

Gelatin is a linear polypeptide that consists of different amounts of 18 amino acids, which is the thermally and hydrolytically denatured product of collagen.[15] It has a triple-helical structure and offers distinctive advantages, such as nontoxicity, remarkable affinity to proteins, commercially available, cheap and environmentally friendly, and is commonly used for pharmaceutical and medical applications because of its biodegradability and biocompatibility in physiological environments. Because the gelatin backbone has abundant amine pendant groups, coming from the amino acids residue, which could be oxidated to nitrite, it could be employed as a reducing reagent based on its mild reductive ability in the synthesis of nanomaterials.[16] Furthermore, the non-polar amino acid chain of the gelatin could immobilize on the surface of graphene through hydrophobic–hydrophobic interactions, which leads to the formation of a stable dispersion of graphene.[17] Therefore, gelatin is selected in the preparation of biocompatible graphene. To the best of our knowledge, no report was found on the use of gelatin both as the reducing reagent and the functionalization reagent in the synthesis of graphene nanosheets.

[a]*Key Lab of Analytical Chemistry for Life Science (MOE), School of Chemistry and Chemical Engineering, Nanjing University, Nanjing, 210093, P. R. China. E-mail: jjzhu@nju.edu.cn; Fax: +86 25 83597204; Tel: +86 25 83597204*
[b]*School of Chemistry and Chemical Engineering, Lanzhou University, Lanzhou, 730000, P. R. China. E-mail: wangcm@lzu.edu.cn; Fax: +86 931 8911895; Tel: +86 931 8911895*

† Electronic supplementary information (ESI) available. See DOI: 10.1039/c1jm10749f

‡ Kunping Liu and Jing-Jing Zhang contributed equally to this work.

Nanomaterial-based drug carriers, such as polymer capsules[18] and carbon nanotubes,[19] have become an important research field due to their efficient drug action, targeted delivery and controlled release of drugs.[20,21] Among them, functionalized carbon nanotubes, as a innovative carrier, has been widely used as the carrier for the delivery of therapeutic molecules due to its large special surface area and being easy to cross cell membranes.[22] The drugs can be loaded through different mechanism, such as embedding, physical absorption and hydrogen bonding interactions.[23,24] Therefore, as a two-dimensional plane structural material, graphene can provide larger specific surface area than other commonly used materials and forms strong π–π conjugation with the drug molecules, which can therefore act as a good candidate for drug loading. Although some efforts have been performed to explore EGO in biological systems,[25,26] few investigation were performed to apply graphene for drug delivery due to its poor solubility and stability in physiological environments. Therefore, it is beneficial to develop novel biocompatible graphene with high solubility and stability in physiological environments.

Herein, a green and facile method for the preparation of gelatin functionalized GNS (gelatin–GNS) with good biocompatibility and physiological stability was reported. Gelatin has both the mild reductive effect to EGO and plays an important role as a functionalized reagent to prevent aggregation. Furthermore, gelatin–GNS was employed as a carrier to load anticancer drugs for cellular uptake and drug delivery (Scheme 1). The result suggested that the gelatin–GNS was nontoxic for MCF-7 cells and experienced a gelatin-mediated sustained release process *in vitro* which has the potential advantage of increasing the therapeutic efficacy. Therefore, the study offers a new avenue to broaden the application of graphene in biomedicine.

2. Experimental

2.1 Materials

Graphite powder (KS-10) and rhodamine 6G (R6G) were from Sigma. Hydrazine hydrate (98%), concentrated sulfuric acid, gelatin (99%), $K_2S_2O_8$ (99%), P_2O_5 (99%) and H_2O_2 (30%) was from Nanjing reagent Co. Ltd. (Nanjing, China) and used as received without further purification. DOX (2 mg mL^{-1}), Dulbecco's modified eagle's medium (DMEM), fetal bovine serum (FBS) and 3-(4, 5-Dimethylthiazol-2-yl)-2, 5-diphenyltetrazolium bromide (MTT) were purchased from Nanjing KeyGen Biotech Co. Ltd. (Nanjing, China). All aqueous solutions were prepared using ultrapure water (18 MΩ) from a Milli-Q system (Millipore).

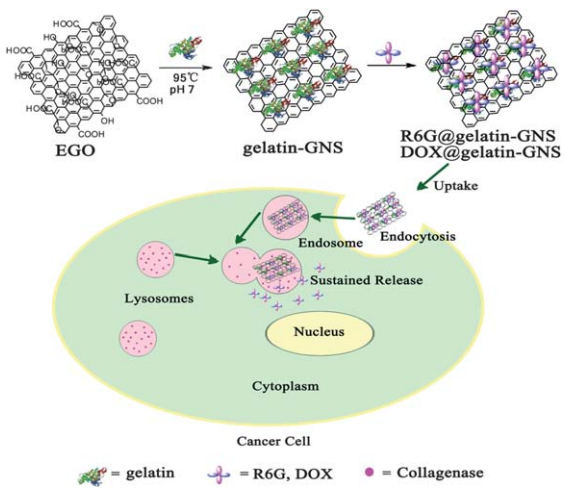

Scheme 1 Illustration of the green synthesis of gelatin–GNS and the possible mechanism of drug delivery as well as gelatin-mediated intracellular sustained release.

2.2 Apparatus

Infrared spectra were collected on a Nicolet 6700 Fourier-transform infrared Spectrometer. UV-vis spectra were obtained from a UV-3600 (Shimadzu) UV-vis Spectrophotometers. HRTEM was performed on a JEOL 2100 high resolution transmission electron microscopy using an accelerating voltage of 200 KV. CLSM image was obtained using a TCS SP5 (Leica) confocal laser scanning microscope. X-Ray powder diffraction (XRD) was performed on a XRD-6000 (Shimadzu) using Cu Kα (1.5406 Å) radiation. AFM was carried out on an agilent 5500 atomic force microscope operated in tapping mode with sample on fleshly cleaved mica. Raman spectra were conducted on a Renishaw in *via* Raman microscope equipped with a ×50 objective with 514.5 nm diode laser excitation on 1800-line grating. Fluorescence spectra were obtained from a RF-5301PC spectroflurophotometer (Shimadzu). Absorbance in MTT assay was recorded at 490 nm using a Bio-Rad 680 microplate reader (USA). Zeta Potential was tested on a nano-z zeta potential analyzer (Malvern). TGA was performed on a STA 449C simultaneous thermal analyzer (Netzsch) from room temperature to 900 °C with a heating rate of 5 °C min^{-1} under a nitrogen atmosphere.

2.3 Preparation of gelatin reduced GNS

Graphite oxide was prepared from graphite powder according to a modified Hummer's method[27] and its concentration was estimated by calibration curve from the absorbance at 231 nm in the UV-vis spectra. In the typical procedure for chemical reduction of EGO to GNS, 1 g of gelatin was first added into 50 mL water, followed by stirring for 0.5 h at 80 °C for the complete dissolution of gelatin. Then a, 50 mL of 0.2 mg mL^{-1}, EGO aqueous dispersion was dropped into the homogeneous gelatin solution at 80 °C. After being vigorously stirred for 30 min, the mixture was allowed to react for 24 h under stirring at about 95 °C. Finally, the resulting stable black dispersion was centrifuged under 20000 rpm and washed three times with hot water to remove excess gelatin. Then, the obtained gelatin stabilized GNS was redispersed in water with a final concentration of 1.0 mg mL^{-1} and stored at 4 °C before further use. Furthermore, as a comparison in a control experiment, pure graphene was also prepared using hydrazine hydrate to reduce the EGO without adding any stabilizer.

2.4 Loading and release of fluorescence probe R6G

To load R6G on gelatin–GNS, 2 mL R6G solution (4 μg mL^{-1}) was incubated with an increasing amount of gelatin–GNS (0, 10, 30, 50, 70, 80, 100, 110, 120 μL) for 2 h under shaking at room

temperature. Then, the mixture was centrifuged at 21000 rpm for 10 min and the supernatant was used to monitor the fluorescence changes of R6G after it was loaded on gelatin–GNS, the fluorescence spectra of R6G were recorded at the wavelength range of 480 to 650 nm using an excitation wavelength of 350 nm. The resulting R6G@gelatin–GNS was stored at 4 °C for further use. The release of R6G from the R6G@gelatin–GNS complex was performed by adding the R6G@gelatin–GNS complex with saturated adsorption of R6G to 2 mL phosphate buffer saline (or acetate buffer solution) at 37 °C with different pH values (7.4, 4.6 and 2.0) or ethanol. After shaking for different time (30, 60, 120, 180, 480 min), the mixture was centrifuged at 21000 rpm for 10 min and the supernatant was used to determine the released R6G following the protocol described above.

2.5 Cellular culture and imaging

In the experiment, Human breast adenocarcinoma (MCF-7) cells were obtained from Nanjing KeyGen Biotech Co. Ltd. A cell culture was performed in a flask in DMEM medium supplemented with 10% (v/v) FBS, penicillin (100 μg mL^{-1}), and streptomycin (100 μg mL^{-1}) in an incubator at 37 °C under a humidified atmosphere containing 5% CO_2. The cells were collected from 90% confluent cell culture plates by aspirating off the media and incubating with trypsin for 3–5 min. Five millilitres of media was added to dilute and neutralize the trypsin solution. Then this solution was separated from the medium by centrifugation at 1000 rpm for 10 min and washed twice with a sterile PBS. The sediment was suspended in the PBS to obtain a homogeneous cell suspension with the final concentration of $\sim 10^7$ cells mL^{-1}. The cell density was determined by using a Petroff–Hausser cell counter (USA) and this was performed prior to the experiment. The cell suspension with various contents was prepared from this stock. For cell imaging, 200 μL of MCF-7 cells ($\sim 10^5$ cell mL^{-1}) were incubated with 20 μL of R6G@gelatin–GNS at 37 °C for 2 h. The R6G@gelatin–GNS concentration in the solution during incubation was ~5 μg mL^{-1}. Cells were washed three times with PBS remove unassociated R6G@gelatin–GNS. Then the cell was observed under CLSM.

2.6 Drug loading and cellular toxicity

Loading of DOX on the gelatin–GNS was carried out using a similar method as R6G loading, except using a DOX concentration of 8 μg mL^{-1} and the volume gradient of gelatin–GNS was 0, 10, 20, 30, 40, 50, 70, 90, 100, 110 and 120 μL, respectively. After centrifugation at 21000 rpm for 10 min, the fluorescence spectra of DOX in the supernatant was recorded to determine the loading amount of DOX using an excitation wavelength of 480 nm under the wavelength range of 500 to 700 nm. The resulting DOX@gelatin–GNS complexes were re-suspended in water and stored at 4 °C. For the cytotoxicity studies, MCF-7 cells were seeded in a 96-well plates with a density of 10^4 cells per well. The cells were incubated in DMEM medium supplemented with 10% (v/v) FBS, penicillin (100 μg mL^{-1}), and streptomycin (100 μg mL^{-1}) at 37 °C under a humidified atmosphere containing 5% CO_2 for 24 h. Then the cell was incubated with different concentration of gelatin–GNS (1, 5, 10, 50, 100, 150, 200 μg mL^{-1}), free DOX (2, 10 μg mL^{-1}) and DOX@gelatin–GNS (2, 10 μg mL^{-1} of DOX) for 24 h and 48 h, respectively. After incubation, cell viability was measured by the MTT assay. Briefly, the media were aspirated and replaced with 90 μL of DMEM medium. To each well 10 μL of MTT stock solution (5 mg mL^{-1}) was added, followed by incubation for 4 h at 37 °C. The supernatant was then removed, and cells were lysed with 200 μL of dimethylsulfoxide. Absorbance was recorded at 490 nm using a Bio-Rad 680 microplate reader.

3. Results and discussion

3.1 Preparation of gelatin–GNS and characterization

A green and one-pot method was used to prepare the high biocompatible graphene nanosheets by using gelatin as a reducing reagent. Briefly, EGO aqueous dispersion was first prepared from natural graphite powder according to the modified method of Hummer.[27] Then, gelatin was used as a reducing reagent for the deoxygenation of EGO. The reduction of the oxo-groups of EGO was confirmed by UV-vis and FTIR spectroscopy as shown in Fig. 1. In the UV-vis spectra, EGO showed a strong absorption at 231 nm and a shoulder at 300 nm, which corresponded to the $\pi \rightarrow \pi^*$ transitions of the aromatic C=C bond and the $n \rightarrow \pi^*$ transition of the C=O bond, respectively. After reduction, the peak at 231 nm was shifted to 266 nm indicating the restoration of the π-conjugation network of the graphene nanosheets. The disappearance of the peak at 300 nm reflected the effect of deoxygenation.[28] As shown in the inset in Fig. 1A, the color change from brown to black in solution before and after reaction was also evident for the reduction of EGO. Because the gelatin–GNS nanosheets were determined to be −31.0 mV by zeta potential, the material could be stably dispersed in water without aggregation after being stored at 4 °C for four months. Furthermore, FT-IR spectroscopy was used to investigate the reduction and functionalization. The spectra of EGO revealed the presence of –OH (3400 cm^{-1}), C=O (1730 cm^{-1}), C=C (1633 cm^{-1}) and C–O (1055 cm^{-1}).[29] After the reduction, the dramatic decrease or disappearance of the adsorption bands of the oxo-groups on graphene and the gelatin–GNS indicated that the EGO was reduced successfully. Moreover, compared with the spectra of gelatin, the characteristic peaks at 2950 cm^{-1}, 1540 cm^{-1}, 1390 cm^{-1}, 1230 +cm^{-1} and 610 cm^{-1} clearly indicated the functionalization of GNS.

The morphology of the gelatin–GNS was observed by TEM, as shown in Fig. 2A, the image exhibited a general view of the graphene nanosheets and clearly illustrated the flake-like shapes

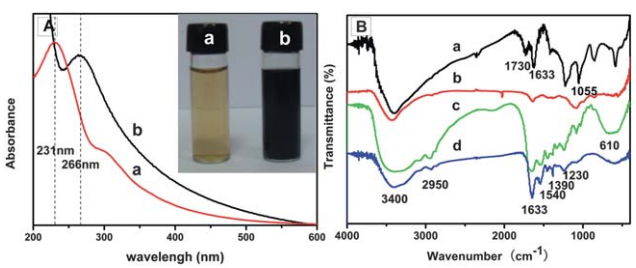

Fig. 1 (A) UV-vis absorption spectra and image (inset) of EGO (0.1 mg mL^{-1}) before (a) and after (b) the reduction with gelatin. (B) FTIR spectra of EGO (a), pure graphene (b), gelatin (c) and gelatin–GNS (d).

of graphene on the plane of which some corrugations and scrolling were also observed. Meanwhile, the as-prepared graphene nanosheets remained separate and no aggregated, indicating that the graphene nanosheets possessed high soluble dispersity. Furthermore, we also analyzed the size distribution of gelatin–GNS through many TEM images. Although most of the large sheets had been removed though centrifugation in preparation process, the little residue of large sheets could not be avoided. The sheets size changed from 80 nm to 3000 nm and approximately 65% of gelatin–GNS sheets are smaller than 750 nm (Fig. S1, ESI†). The XRD pattern was investigated as shown in Fig. 2B to monitor the synthetic process and the reaction completion for the oxidation of graphite and the reduction of EGO. It showed a disappearance of characteristic diffraction peak of graphite at 26.4° indicating the complete oxidation of graphite. Meanwhile, a new peak was observed at 10.0° when graphite was oxidized to GO, which was due to the intercalation of oxo-groups to the interlayer of carbon sheets. After the reduction, no obvious peak was observed in the gelatin–GNS, indicating the complete reduction of EGO.

Atomic force microscopy (AFM) was used to characterize the morphology and thickness of the graphene. Fig. 3 showed in the representative AFM images and cross-section analyses along with the line in AFM images of EGO and gelatin–GNS. The EGO nanosheets had a mean thickness of about 0.8 nm, which was larger than the theoretical value of graphene sheet because of the presence of covalently bound oxo-groups.[30] After the reduction, the thickness of the obtained gelatin–GNS increased to about 3.0 nm, which was similar to that of the graphene using bovine serum albumin (BSA) as the reducing reagent.[14] Although most oxo-groups were removed after the reduction, the thicker gelatin–GNS could be attributed to the attachment of gelatin. Furthermore, as could be observed, the functionalization of gelatin could prevent the GNS agglomeration, because most of the negative gelatin–GNS was kept independent from each other in the dispersion based on the electrostatic interaction. Therefore, the gelatin could not only act as a reducing reagent, but also plays an important role as a capping reagent for the stabilization of the gelatin–GNS.

In order to confirm the single sheet nature of the gelatin–GNS, Raman spectra were used to investigate the graphite, EGO, pure graphene and gelatin–GNS. Generally, the Raman spectra of graphene exhibited four main feature peaks. D band was attributed to a breathing mode of κ-point photons of A_{1g} symmetry mode activated by the presence of disorder (about 1350 cm^{-1}) and the G band arisen from the first order scattering of the E_{2g} phonon of C sp^2 atoms (about 1575 cm^{-1}). The 2D band represented the symmetry-allowed overtone of the G band. The shift and shape of the 2D peak depended on the number of graphene layers in which single-layer graphene had a single, sharp 2D peak below 2700 cm^{-1} while bilayer or more sheets had a broader and upshifted 2D peak located at about or more than 2700 cm^{-1}. The cooperation between D and G peaks gives rise to a D + G combination band induced by disorder at about 2930 cm^{-1}, indicating the presence of highly disordered and randomly arranged graphene sheets.[31] The representative Raman spectra were shown in Fig. 4A, in which graphite showed a sharp G band at 1575 cm^{-1} in relation to the in-phase vibration of the graphite lattice and a broad 2D peak at 2720 cm^{-1}. Moreover, a weak D band was also found at 1350 cm^{-1}. After the oxidation, EGO showed a broad and blue shifted G band at 1585 cm^{-1}, attributing to the presence of isolated double bonds which resonate at higher frequencies than the G band of graphite.[32] The intensity of D band at 1350 cm^{-1} was significantly increased compared with graphite, indicating the decrease in the size of the in-plane sp^2 domains. Both the pure graphene and gelatin–GNS exhibited a D band at the same position with EGO and also a broad G band at 1595 cm^{-1}. Furthermore, the high energy second-order 2D band at 2681 cm^{-1} and the D + G combination mode at 2930 cm^{-1} were also observed in the Raman spectra of EGO, pure graphene and gelatin–GNS. The shape and the shift lower than 2700 cm^{-1} of the 2D band indicated that the as-prepared gelatin–GNS were a single layer crystal structure and the increase in thickness of the gelatin-G must completely come from the attachment of gelatin.

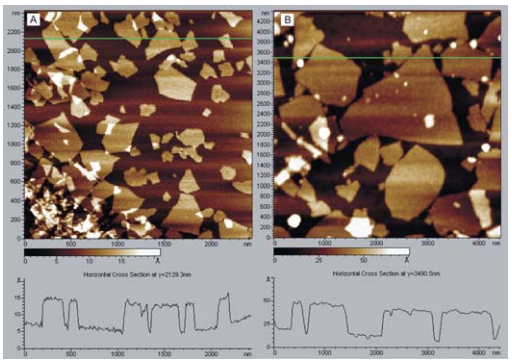

Fig. 3 Typical AFM images and cross-section analysis along with the line in AFM images of EGO (A) and gelatin-G (B).

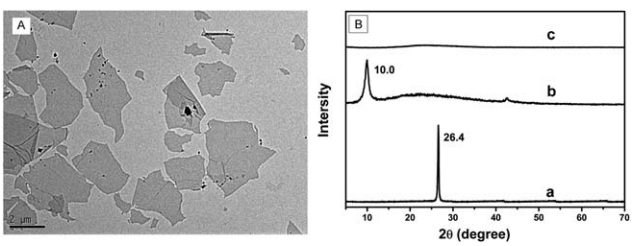

Fig. 2 (A) Typical TEM image of gelatin–GNS. (B) XRD patterns of graphite (a), EGO (b) and gelatin–GNS (c).

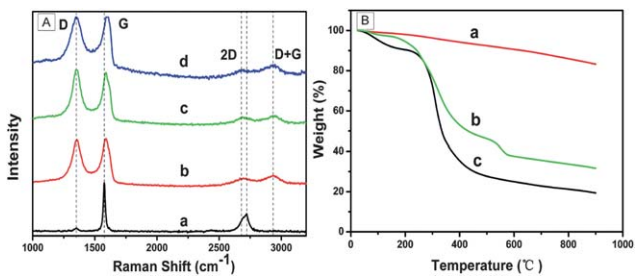

Fig. 4 (A) Raman spectra of graphite (a), EGO (b), pure graphene (c) and gelatin–GNS (d). (B) TGA curves of pure graphene (a), gelatin–GNS (b) and gelatin (c).

The thermal behavior of the gelatin, pure graphene and gelatin–GNS was also investigated by thermal gravimetric analysis (TGA), in a nitrogen atmosphere, to verify the functionalization. As shown in Fig. 4B, the pure graphene exhibited a small mass loss of about 15 wt% at full temperature range, indicating a good thermal stability. The gelatin exhibited about 10 wt% losses below 200 °C, resulting from the removal of the labile oxo-groups, such as CO, CO_2, and H_2O vapors, and about 60 wt% losses below 400 °C by the decomposition of gelatin.[33] The gelatin–GNS also exhibited about 3 wt% losses below 200 °C and about 45 wt% losses below 400 °C. However, it also exhibited about a 10 wt% losses below 600 °C due to the bulk pyrolysis of the carbon skeleton.[13]

For biomedical use, graphene nanosheets should be stable in both buffer solution and the various physiological environments. Low concentration of salts in the medium might increase the agglomerates of carbon nanomaterials.[34] Therefore, the stability of EGO and gelatin–GNS was investigated by incubating them in PBS (0.01M), cellular growth media as well as serum for 24 h. As shown in Fig. 5, the EGO with the concentration of 0.2 mg mL^{-1} was soluble and stable in water but substantially aggregated in PBS and DMEM cell growth medium and slightly aggregated in fetal bovine serum (FBS). This might be the electrostatic and salt effect to brake the equilibrium state of EGO in solution. However, the gelatin–GNS with the same concentration exhibited an excellent stability and no aggregation was observed in 24 h. This phenomenon implied that the attachment of gelatin could tailor the nanocomposite properties and also provided long-term stability by effectively preventing agglomeration of graphene in various physiological fluids that contained various proteins and other organic molecules as well as high salt concentration. Therefore, the gelatin–GNS possessed a good biocompatibility and stability to act as an ideal alternation for potential biological applications, such as cellular imaging and drug delivery.

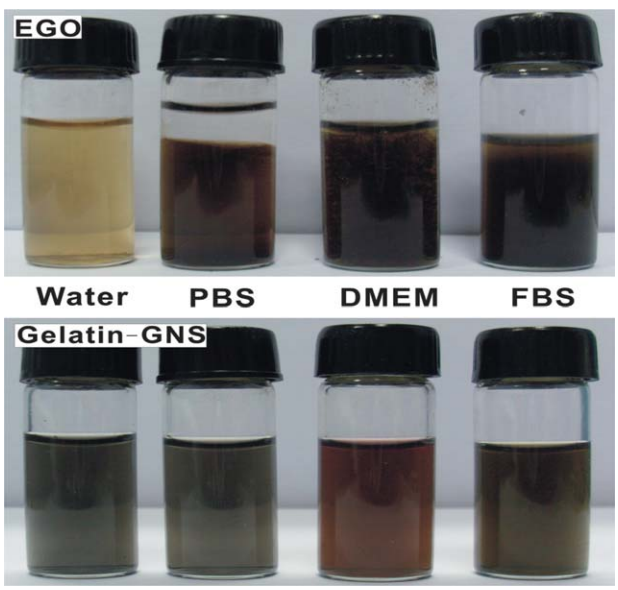

Fig. 5 Photo images of EGO (A) and gelatin–GNS (B) in various physiological fluids.

3.2 Loading and release of R6G

To understand the cellular uptake of the gelatin–GNS as a drug carrier, R6G was selected as the model fluorescence probe to label gelatin–GNS. As a commonly used model drug, R6G was a cationic dye that could bind with negatively charged gelatin–GNS to form R6G@gelatin–GNS complex as a result of electrostatic attraction. The loading process was monitored by measuring the fluorescence quenching of R6G at about 550 nm by using an excitation wavelength of 350 nm upon the addition of increasing quantities (from 0 to 120 μL) of gelatin–GNS.[35] As shown in Fig. 6A, with the increase of gelatin–GNS, the fluorescence intensity of R6G in supernatant decreased gradually, which indicated that the fluorescence quenching might be the result of non-radiative energy transfer between excited R6G and the surface of the nanoparticles.[36] The observation provided the evidence for R6G loading on the surface of gelatin–GNS. Maximum quench was attained at 110 μL of gelatin–GNS (1 mg mL^{-1}), indicating the saturated adsorption of gelatin–GNS toward R6G. The loading capacity could be calculated to be 8 μg of R6G to 110 μg of gelatin–GNS, which was higher than other materials reported.[37,38] This high loading capacity was due to the large specific surface area and the strong π–π conjugation as well as hydrogen bonding interactions between gelatin–GNS and R6G.

To measure the release kinetics, R6G@gelatin–GNS was dispersed in a buffer solution with various pH. Fig. 6B showed the pH-dependent R6G release kinetics. Regardless of the pH value, R6G@gelatin–GNS exhibited sustained release properties with a relatively fast release at the initial stage. Furthermore, the release amount of R6G at pH 3.0 was different. At pH 7.4, the release rate was very slow and only about 5% of the total amount was released over 8 h. However, the release behavior at acidic conditions indicated that the total releasing amount of R6G

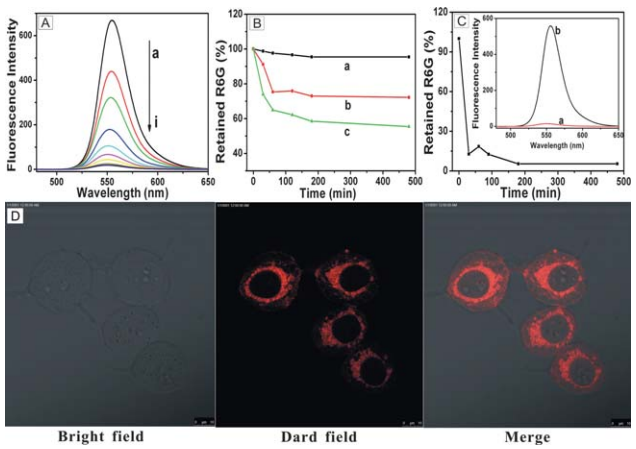

Fig. 6 (A) Fluorescence spectra of R6G solution (8 μg in 2 mL of water) with increasing amounts of gelatin–GNS with a concentration of 1.0 mg mL^{-1} (from a to i: 0, 10, 30, 50, 70, 80, 100, 110, 120 μL) using the excitation wavelength of 350 nm. (B) R6G release profiles for R6G@gelatin–GNS measured in PBS (or acetate buffer) at pH 7.4 (a), 4.6 (b) and 2.0 (c) at 37 °C. (C) R6G release profiles for R6G@gelatin–GNS measured in ethanol and the fluorescence spectra of R6G@gelatin–GNS in water (a) and after treatment with ethanol (b). (D) CLSM images of MCF-7 cells for incubation with R6G@gelatin–GNS for 2 h at 37 °C.

within the same time was much higher than that at pH 7.4. About 28% and 45% of the total bound R6G was released from the R6G@gelatin–GNS at pH 4.6 and 2.0, respectively. The results might be ascribed to the partial dissociation of the hydrogen bonding interactions between R6G and gelatin–GNS under acid conditions.[32] This pH-dependent drug release from the gelatin–GNS is important for clinical medicine, since the microenvironments in extracellular tissues of tumors and intracellular lysosomes and endosomes were acidic, which differ from the common body fluid with pH 7.4. This could activate the drug release from the gelatin–GNS.[39] Furthermore, the release behavior of R6G@gelatin–GNS in ethanol was also investigated as shown in Fig. 6C. Surprisingly, a fast release of about 90% of the total amount was observed. Moreover, as shown in the inset of Fig. 6C, the R6G@gelatin–GNS complex exhibited complete fluorescence quenching, which might come from the fluorescence resonance energy transfer from the dye to the gelatin–GNS. Therefore, this efficient quenching implied the presence of strong π–π stacking interactions between R6G and gelatin–GNS except for the electrostatic attraction and hydrogen bonding. After treated with ethanol, the fluorescence of R6G@gelatin–GNS was recovered, indicating the desorption of R6G from gelatin–GNS in the presence of ethanol, which was due to the higher solubility of R6G in ethanol compared to water, as well as hydrophobic interactions and the dissociation of the hydrogen bonding interactions between R6G and the gelatin–GNS. The result led to the good release but poor uptake properties of R6G in ethanol.[40] However, it was interesting that this phenomenon might be useful for cell imaging because there were a lot of organic compound, such as glycans, protein and lipide in the cells, which might induce the fluorescence recovery of R6G@gelatin–GNS, similar to previous reports.[25,26]

3.3 Cellular uptake and cytotoxicity

The R6G@gelatin–GNS complex was then incubated with MCF-7 cells and the cells were observed using confocal laser scanning microscopy (CLSM). As shown in Fig. 6D, intense R6G red fluorescence with little background was observed in the cytoplasm surrounding the nucleus, which was associated with the uptake of R6G@gelatin–GNS into the cytoplasm and also onto the membrane of the cells. Since the fluorescence of R6G was significantly quenched when loaded on gelatin–GNS, the appearance of fluorescence inside the cells indicated the actual release of R6G from gelatin–GNS as expected due to the interaction with the cells. This phenomenon indicated that the R6G@gelatin–GNS could be effectively internalized by MCF-7 cells within 2 h resided mainly in the cytoplasm. Therefore, the R6G@gelatin–GNS might be taken up by the MCF-7 cell through a nonspecific endocytosis mechanism,[41–43] after which the R6G molecules were released in endocytic compartments (*i.e.*, endosomes and later lysosomes) and the fluorescence of R6G@gelatin–GNS was recovered.[44]

To evaluate the performance of drug loading and the cellular toxicity of gelatin–GNS, doxorubicin (DOX), a commonly used anticancer drug, was loaded on gelatin–GNS to form the DOX@gelatin–GNS complex using the similar method as R6G@gelatin–GNS. According to the maximum fluorescence quench of DOX at 120 μL of gelatin–GNS, as shown in Fig. 7A, the saturated adsorption of gelatin–GNS toward DOX was 16 μg of DOX to 120 μg of gelatin–GNS, which was larger than iron oxide nanoparticles and hollow chitosan/poly(acrylic acid) nanospheres.[35,45] The high loading capacity of DOX was useful in clinic medicine application because it could increase the efficacy of drug. Therefore, the gelatin–GNS was expected to be an excellent candidate material for use as intracellular drug vehicles for clinic cancer therapy.

Then the MCF-7 cells were exposed to a series of different concentrations with gelatin–GNS, free DOX, and DOX@gelatin–GNS for 24 h and 48 h, respectively. The relative cellular viabilities were determined using the MTT method. As shown in Fig. 7B, no obvious cytotoxicity against MCF-7 cells was found for the gelatin–GNS even at a high concentration of 200 μg mL^{-1}. In fact, the dosage of gelatin–GNS adopted in the all cellular cytotoxicity experiment was much lower than 200 μg mL^{-1}. According to the size distribution of the gelatin–GNS sheets, the concentration of gelatin–GNS sheets smaller than 750 nm was estimated to be about 90 μg mL^{-1} when the total concentration of gelatin–GNS was 200 μg mL^{-1}. It means that the MCF-7 cells still maintained high activity when the concentration of small size gelatin–GNS changed from 0 to 90 μg mL^{-1}. Thus, although there were some larger sheets in the gelatin–GNS, the smaller size sheets would be the main participants in the drug delivery process and showed very low cytotoxicity against MCF-7 cell. The cytotoxicity of the DOX@gelatin–GNS compared with that of free DOX was shown in Fig. 7C. As could be seen, with the increase of time, the cytotoxicity of both DOX@gelatin–GNS and free DOX enhanced gradually. Additionally, the DOX@gelatin–GNS exhibited lower cytotoxicity compared with free DOX at the same dose. The lower cytotoxicity of DOX@gelatin–GNS indicated that the release of DOX from DOX@gelatin–GNS might experience a sustained release process due to a time-consuming DOX release. The possible mechanism of sustained release was speculated as follows and shown in Scheme 1: after the endocytosis of cancer cell, the DOX@gelatin–GNS was encapsulated in endsome and then merged with lysosome, which contained many kinds of hydrolase, such as phosphatase, cathepsin and collagenase.[46,47] With the degradation effect of collagenase to gelatin on the GNS,[48,49] the DOX was released gradually from the GNS and then exhibited a sustained release effect. This gelatin-mediated sustained release effect of the drug was much more useful for cancer therapy in clinic application because it could control the release

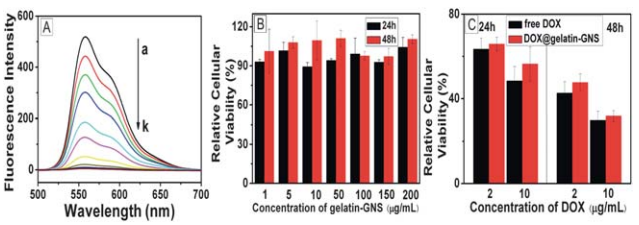

Fig. 7 (A) Fluorescence spectra of DOX solution (16 μg in 2 mL of water) with increasing amounts of gelatin–GNS with a concentration of 1.0 mg mL^{-1} (from a to k: 0, 10, 20, 30, 40, 50, 70, 90, 100, 110, 120 μL) using the excitation wavelength of 350 nm. (B) Relative cell viability of MCF-7 cells treated with different concentration of gelatin-G after 24 h and 48 h incubation. (C) Cytotoxicity of free DOX and DOX@gelatin-G to MCF-7 cells after 24 h and 48 h incubation.

rate of drug in body so that the blood drug concentration could be maintained at a stable concentration for a long time, thus enhancing the therapeutic efficacy. Therefore, the as-prepared gelatin–GNS was nontoxic and showed high loading capacity for drugs so that it could be used as an ideal nanocarrier for drug delivery.

4. Conclusions

In summary, a green and facile synthetic approach of GNS based on gelatin was reported by using EGO as a precursor, in which gelatin acted as not only a reducing reagent but also a functionalization reagent. The obtained biocompatible gelatin–GNS showed high aqueous solubility and stability in various physiological fluids. Additionally, it exhibited a high drug loading capacity due to the large special surface area and strong π–π conjugation. Therefore, the material was used to study the cellular imaging and drug delivery, which suggested that it was nontoxic and might be taken up by MCF-7 cells through a nonspecific endocytosis mechanism. Therefore, it could act as an ideal carrier for drug delivery. Moreover, the release of DOX from DOX@gelatin–GNS in the cells likely experienced a gelatin-mediated sustained release process, which may have potential clinical advantages pertaining to increased therapeutic efficacy. The present strategy definitely paves a way for the preparation of graphene with good biocompatibility and solubility, thus providing a novel and promising platform for the study of the biological applications of graphene.

Acknowledgements

The authors acknowledge the support of National Natural Science Foundation of China (Nos. 20635020, 20775030, 20821063). This work is also supported by 973 Program (No: 2011CB933502).

References

1 K. S. Novoselov, A. K. Geim, S. V. Morozov, D. Jiang, Y. Zhang, S. V. Dubonos, I. V. Grigorieva and A. A. Firsov, *Science*, 2004, **306**, 666.
2 F. N. Xia, D. B. Farmer, Y. M. Lin and P. Avouris, *Nano Lett.*, 2010, **10**, 715.
3 Q. Wu, Y. X. Xu, Z. Y. Yao, A. R. Liu and G. Q. Shi, *ACS Nano*, 2010, **4**, 1963.
4 H. X. Chang, L. H. Tang, Y. Wang, J. H. Jiang and J. H. Li, *Anal. Chem.*, 2010, **82**, 2341.
5 D. Li, M. B. Muller, S. Gilje, R. B. Kaner and G. G. Wallace, *Nat. Nanotechnol.*, 2008, **3**, 101.
6 A. Reina, X. T. Jia, J. Ho, D. Nezich, H. Son, V. Bulovic, M. S. Dresselhaus and J. Kong, *Nano Lett.*, 2009, **9**, 30.
7 L. Y. Jiao, L. Zhang, X. R. Wang, G. Diankov and H. J. Dai, *Nature*, 2009, **458**, 877.
8 C. S. Shan, H. F. Yang, J. F. Song, D. X. Han, A. Ivaska and L. Niu, *Anal. Chem.*, 2009, **81**, 2378.
9 S. Stankovich, R. D. Piner, X. Q. Chen, N. Q. Wu, S. T. Nguyen and R. S. Ruoff, *J. Mater. Chem.*, 2006, **16**, 155.
10 K. P. Liu, J. J. Zhang, G. H. Yang, C. M. Wang and J. J. Zhu, *Electrochem. Commun.*, 2010, **12**, 402.
11 W. Lv, M. Guo, M. H. Liang, F. M. Jin, L. Cui, L. J. Zhi and Q. H. Yang, *J. Mater. Chem.*, 2010, **20**, 6668.
12 J. L. Zhang, H. J. Yang, G. X. Shen, P. Cheng, J. Y. Zhang and S. W. Guo, *Chem. Commun.*, 2010, **46**, 1112.
13 C. Z. Zhu, S. J. Guo, Y. X. Fang and S. J. Dong, *ACS Nano*, 2010, **4**, 2429.
14 J. B. Liu, S. H. Fu, B. Yuan, Y. L. Li and Z. X. Deng, *J. Am. Chem. Soc.*, 2010, **132**, 7279.
15 N. Li, J. Z. Xu, H. Yao, J. J. Zhu and H. Y. Chen, *J. Phys. Chem. B*, 2006, **110**, 11561.
16 J. J. Zhang, M. M. Gu, T. T. Zheng and J. J. Zhu, *Anal. Chem.*, 2009, **81**, 6641.
17 W. Zheng and Y. F. Zheng, *Electrochem. Commun.*, 2007, **9**, 1619.
18 J. Liu, Y. Zhang, C. Y. Wang, R. Z. Xu, Z. P. Chen and N. Gu, *J. Phys. Chem. C*, 2010, **114**, 7673.
19 A. Bianco, K. Kostarelos, C. D. Partidos and M. Prato, *Chem. Commun.*, 2005, 571.
20 S. Santra, C. Kaittanis, J. Grimm and J. M. Perez, *Small*, 2009, **5**, 1862.
21 W. Wei, G. H. Ma, G. Hu, D. Yu, T. Mcleish, Z. G. Su and Z. Y. Shen, *J. Am. Chem. Soc.*, 2008, **130**, 15808.
22 W. Wu, S. Wieckowski, G. Pastorin, M. Benincasa, C. Klumpp, J. P. Briand, R. Gennaro, M. Prato and A. Bianco, *Angew. Chem., Int. Ed.*, 2005, **44**, 6358.
23 K. N. J. Burger, R. W. H. M. Staffhorst, H. C. D. Vijlder, M. J. Velinava, P. H. Bomans, P. M. Frederik and B. D. Kruijff, *Nat. Med.*, 2002, **8**, 81.
24 Z. Liu, X. M. Sun, N. Nakayama-Ratchford and H. J. Dai, *ACS Nano*, 2007, **1**, 50.
25 Z. Liu, J. T. Robinson, X. M. Sun and H. J. Dai, *J. Am. Chem. Soc.*, 2008, **130**, 10876.
26 L. M. Zhang, J. G. Xia, Q. H. Zhao, L. W. Liu and Z. J. Zhang, *Small*, 2010, **6**, 537–544.
27 W. S. Hummers and R. E. Offeman, *J. Am. Chem. Soc.*, 1958, **80**, 1339.
28 Y. Zhou, Q. L. Bao, L. A. L. Tang, Y. L. Zhong and K. P. Loh, *Chem. Mater.*, 2009, **21**, 2950.
29 C. S. Shan, H. F. Yang, D. X. Han, Q. X. Zhang, A. Ivaska and L. Niu, *Langmuir*, 2009, **25**, 12030.
30 S. Stakovich, D. A. Dikin, R. D. Piner, K. A. Kohlhaas, A. Kleinhammes, Y. Y. Jia, Y. Wu, S. T. Nguyen and R. S. Ruoff, *Carbon*, 2007, **45**, 1558.
31 A. C. Ferrari, J. C. Meyer, V. Scardaci, C. Casiraghi, M. Lazzeri, F. Mauri, S. Piscanec, D. Jiang, K. S. Novoselov, S. Roth and A. K. Geim, *Phys. Rev. Lett.*, 2006, **97**, 187401.
32 K. N. Kudin, B. Ozbas, H. C. Schniepp, R. K. Prudhomme, I. A. Aksay and R. Car, *Nano Lett.*, 2008, **8**, 36.
33 M. A. Rahman, M. A. Khan and S. M. Tareq, *J. Appl. Polym. Sci.*, 2010, **117**, 2075.
34 M. Sano, J. Okamura and S. Shinkai, *Langmuir*, 2001, **17**, 7172.
35 M. K. Yu, Y. Y. Jeong, J. Park, S. Park, J. W. Kim, J. J. Min, K. Kim and S. Jon, *Angew. Chem., Int. Ed.*, 2008, **47**, 5362.
36 L. Josephson, M. F. Kircher, U. Mahmood, Y. Tang and R. Weissleder, *Bioconjugate Chem.*, 2002, **13**, 554.
37 S. H. Liu, R. M. Xing, F. Lu, R. K. Rana and J. J. Zhu, *J. Phys. Chem. C*, 2009, **113**, 21042.
38 P. Guo, C. R. Martin, Y. P. Zhao, J. Ge and R. N. Zare, *Nano Lett.*, 2010, **10**, 2202.
39 X. M. Sun, Z. Liu, K. Welsher, J. T. Robinson, A. Goodwin, S. Zaric and H. J. Dai, *Nano Res.*, 2008, **1**, 203.
40 B. Yu, D. A. Wang, Q. Ye, F. Zhou and W. M. Liu, *Chem. Commun.*, 2009, (44), 6789.
41 L. M. Bareford and P. W. Swaan, *Adv. Drug Delivery Rev.*, 2007, **59**, 748.
42 H. Hacker, H. Mischak, T. Miethke1, S. Liptay, R. Schmid, T. Sparwasser, K. Heeg, G. B. Lipford and H. Wagner, *EMBO J.*, 1998, **17**, 6230.
43 R. Guo, R. T. Li, X. L. Li, L. Y. Zhang, X. Q. Jiang and B. R. Liu, *Small*, 2009, **5**, 709.
44 W. L. Zhang, Y. L. Li, L. X. Liu, Q. Q. Sun, X. T. Shuai, W. Zhu and Y. M. Chen, *Biomacromolecules*, 2010, **11**, 1331.
45 Y. Hu, Y. Ding, D. Ding, M. J. Sun, L. Y. Zhang, X. Q. Jiang and C. Z. Yang, *Biomacromolecules*, 2007, **8**, 1069.
46 C. D. Duve and R. Wattiaux, *Annu. Rev. Physiol.*, 1966, **28**, 435.
47 V. Everts, W. Korper, A. Niehof, I. Jansen and W. Beertsen, *Matrix Biol.*, 1995, **14**, 665.
48 T. Tanigo, R. Takaoka and Y. J. Tabata, *J. Controlled Release*, 2010, **143**, 201.
49 Y. B. Choy, F. Cheng, H. Choi and K. Kim, *Macromol. Biosci.*, 2008, **8**, 758.

